CDDpress

www.nature.com/cdd

ARTICLE

TRIM21 regulates pyroptotic cell death by promoting Gasdermin D oligomerization

Wenqing Gao[1,10], Yuanyuan Li[1,10], Xuehe Liu[1], Sen Wang[1], Pucheng Mei[1], Zijun Chen[1], Kewei Liu[2], Suhua Li[3], Xue-Wei Xu[4], Jianhua Gan[5], Jiaxue Wu[5], Chaoneng Ji[5], Chen Ding[5], Xing Liu[6], Yuping Lai[2], Housheng Hansen He[7], Judy Lieberman[6], Hao Wu[8], Xiangjun Chen[9]✉ and Jixi Li[1]✉

Gasdermin-D (GSDMD), the executioner of pyroptotic cell death when it is cleaved by inflammatory caspases, plays a crucial role in host defense and the response to danger signals. So far, there are no known mechanisms, other than cleavage, for regulating GSDMD. Here, we show that tripartite motif protein TRIM21 acts as a positive regulator of GSDMD-dependent pyroptosis. TRIM21 interacted with GSDMD via its PRY-SPRY domain, maintaining GSDMD stable expression in resting cells yet inducing the N-terminus of GSDMD (GSDMD-N) aggregation during pyroptosis. TRIM21-deficient cells displayed a reduced cell death in response to NLRP3 or NLRC4 inflammasome activation. Genetic ablation of TRIM21 in mice conferred protection from LPS-induced inflammation and dextran sulfate sodium-induced colitis. Therefore, TRIM21 plays an essential role in GSDMD-mediated pyroptosis and may be a viable target for controlling and treating inflammation-associated diseases.

Cell Death & Differentiation; https://doi.org/10.1038/s41418-021-00867-z

INTRODUCTION

Pyroptosis has been characterized as a form of regulated cell death [1] initiated by inflammasome activation; it plays critical roles in the host defense against danger signals [2]. Similar to cell necroptosis, which is induced by receptor-interacting protein kinase 1 (RIPK1)/RIPK3/mixed lineage kinase domain-like (MLKL) via the tumor necrosis factor receptor or other stimuli [3–5], pyroptosis is typically considered a highly pro-inflammatory type of cell death. To avoid damage to the host, the activation of inflammatory caspases (human and mouse caspase-1, or murine caspase-11 and its human homologs caspase-4 and 5) preceding pyroptosis is tightly regulated [6, 7]. These inflammatory caspases are activated within inflammasomes, multi-protein complexes that are assembled upon the detecting of pathogen- or damage-associated molecular patterns [8, 9].

Gasdermin D (GSDMD) is a central executioner of pyroptotic cell death downstream of both caspase-1 and caspase-11 [6, 7]. Human GSDMD is composed of two domains: the N-terminal domain (residues 1–275, hereafter GSDMD-N) and the C-terminal domain (residues 276–484, hereafter GSDMD-C). GSDMD-N binds lipids and forms ring-like structures within membranes that function as pores to facilitate the release of interleukin-1β (IL-1β), as well as to trigger pyroptosis [8, 10–14]. GSDMD-C functions in an auto-inhibitory manner to help stabilize the full-length GSDMD [15, 16]. During pathogenic *Yersinia* infection, there is an alternate pyroptotic pathway mediated by Toll-like receptors or death receptors that recruit caspase-8, which cleaves GSDMD at Asp276 and then induces pyroptosis. Downstream of caspase-8, caspase-3 inactivates GSDMD by clevage the full-length protein or GSDMD-N at Asp88 [17]. In hyperactive macrophages, GSDMD pores are required for IL-1β release in a non-pyroptotic context [18], indicating that damage to the plasma membrane does not necessarily result in cell death. Moreover, the endosomal sorting complexes required for transport (ESCRT) machinery can repair GSDMD-induced membrane rupture via calcium influx signals to rescue pyroptosis [19].

Tripartite motif (TRIM)-containing proteins control essential cellular processes such as innate immunity, transcription, autophagy, and carcinogenesis [20]. TRIM21, a TRIM protein family member, is initially identified as an autoantigen in autoimmune diseases such as rheumatoid arthritis, systemic lupus erythematosus, and Sjorgen's syndrome [21]. TRIM21 possesses E3 ligase activity and can promote the innate immune response to RNA viral infection through K27-linked polyubiquitination of MAVS [22], and plays an essential role in redox regulation by directly

[1]Department of Neurology, Huashan Hospital and Institute of Neurology, State Key Laboratory of Genetic Engineering, School of Life Sciences, MOE Engineering Research Center of Gene Technology, Shanghai Engineering Research Center of Industrial Microorganisms, Fudan University, Shanghai, China. [2]Shanghai Key Laboratory of Regulatory Biology, School of Life Sciences, East China Normal University, Shanghai, China. [3]Division of Natural Science, Duke Kunshan University, Suzhou, Jiangsu, China. [4]Key Laboratory of Marine Ecosystem Dynamics, Ministry of Natural Resources & Second Institute of Oceanography, Ministry of Natural Resources, Hangzhou, China. [5]State Key Laboratory of Genetic Engineering, School of Life Sciences, Fudan University, Shanghai, China. [6]Program in Cellular and Molecular Medicine, Boston Children's Hospital and Department of Pediatrics, Harvard Medical School, Boston, MA, USA. [7]Department of Medical Biophysics, University of Toronto, and Princess Margaret Cancer Center, University Health Network, Toronto, ON, Canada. [8]Program in Cellular and Molecular Medicine, Boston Children's Hospital and Department of Biological Chemistry and Molecular Pharmacology, Harvard Medical School, Boston, MA, USA. [9]Department of Neurology, Huashan Hospital and Institute of Neurology, Fudan University, Shanghai, China. [10]These authors contributed equally: Wenqing Gao, Yuanyuan Li. ✉email: xiangjchen@fudan.edu.cn; lijixi@fudan.edu.cn

Edited by V.M. Dixit

Received: 9 February 2021 Revised: 31 August 2021 Accepted: 31 August 2021
Published online: 11 September 2021

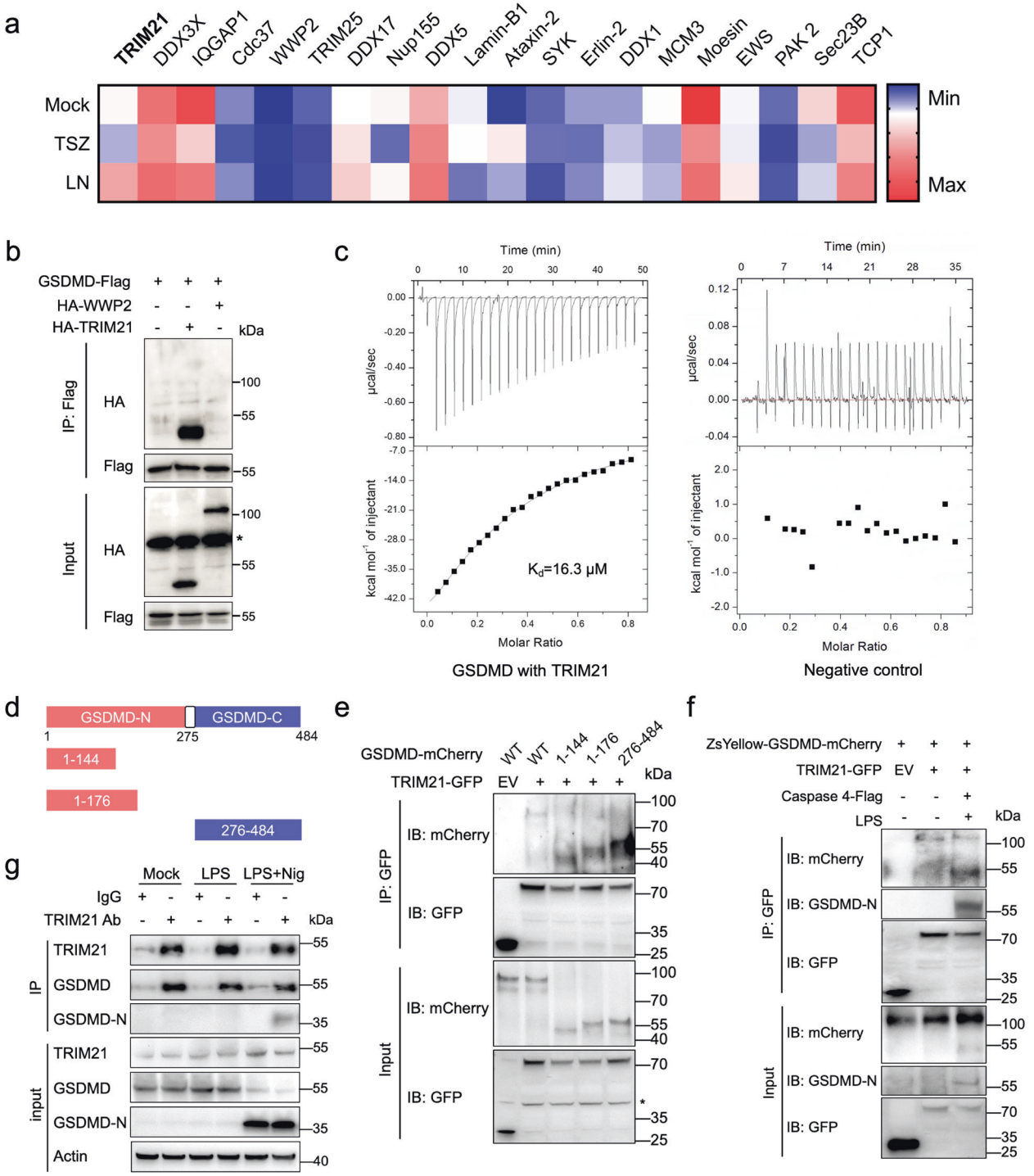

interacting with SQSTM1/p62 and ubiquitylating p62 at its K7 residue via K63-linkage [23].

Although GSDMD has emerged as a new cell death executioner, little is known about the precise regulatory mechanism, or how GSDMD is triggered to form pore-like structures in membranes. In this report, we identified TRIM21 as an interacting protein of GSDMD and found that TRIM21 promoted the formation of GSDMD-N aggregates, thus contributing to pyroptotic cell death. The PRY-SPRY domain of TRIM21 rather than its RING domain, which possesses E3 ligase activity, is essential for modulating pyroptosis. Besides, TRIM21 deficiency attenuated the severity of LPS-induced inflammation and DSS-induced colitis by suppressing GSDMD-N activity.

RESULTS

TRIM21 directly interacts with GSDMD

To identify the potential factors that regulate GSDMD oligomerization and the formation of pore-like structures in the cell membrane, we performed high-sensitivity mass spectrometry by immunoprecipitating the endogenous GSDMD protein in immortalized bone marrow-derived macrophages (iBMDMs) with GSDMD antibody. Over 13,000 peptides were screened, and one TRIM family protein TRIM21 was found to possibly be associated with GSDMD in LPS plus nigericin (Nig)-induced pyroptosis but not in TSZ-induced necroptosis (Fig. 1a). When Flag-tagged GSDMD was co-transfected with HA-tagged TRIM21 into

Fig. 1 GSDMD directly interacts with TRIM21. a Heatmap depicts the levels of proteins identified by mass spectrometry that might interact with GSDMD in iBMDMs treated with or without TSZ (10 ng/mL TNF-α, 100 nM Smac, and 10 μM ZVAD) and LPS plus Nig (iBMDMs were primed with 1 μg/mL LPS for 2 h and then stimulated with 20 μM Nig for 30 min). Immunocomplexes of endogenous GSDMD were subjected to SDS-PAGE. Gels were cut based on heavy-chain IgG bands. The sample was analyzed as described previously [49]. **b** Co-immunoprecipitation (Co-IP) analysis of GSDMD-Flag with HA-TRIM21 or HA-WWP2 in HEK293T cells. Asterisk (*) symbol indicates, nonspecific binding. **c** Measurements of the binding affinity between GSDMD and TRIM21 or WWP2 (negative control) by ITC method. The upper panel represents the raw data, revealing the calorimetric response peaks in μWatt during successive injections of GSDMD to the TRIM21 sample cell or the WWP2 sample cell. Individual peaks from titrations were integrated and presented in a Wiseman plot. The lower panel is the best fit of the raw data after subtracting the heat of dilution from the appropriate buffer blank. The solid line in the lower panel shows the best fit of the raw data to the one-set of sites binding model. Apparent K_d of GSDMD to TRIM21 was 16.3 ± 1.8 μM. Titrations were carried out at 25 °C in 20 mM Tris-HCl buffer (pH 8.0) containing 150 mM NaCl. **d** The schematic diagram of human GSDMD and its truncated mutants. **e** GSDMD-mCherry or its mutants and TRIM21-GFP were co-transfected into HeLa cells. Lysates were immunoprecipitated with anti-GFP antibody and then immunoblotted with anti-mCherry or anti-GFP antibody. Asterisk (*) symbol indicates nonspecific binding. EV empty vector. **f** HEK293T cells were transfected with ZsYellow-GSDMD-mCherry, Caspase-4-Flag, and TRIM21-GFP as described. The cells were transfected with 1 μg/mL LPS and incubated at 37 °C for 4 h. Anti-GFP agarose beads were used in the following co-IP analysis. **g** Endogenous GSDMD binds with TRIM21 in mouse primary BMDMs. BMDM cell lysates were immunoprecipitated with an anti-TRIM21 antibody or IgG as control, followed by anti-GSDMD or anti-TRIM21 immunoblotting. All data are representative of three independent experiments.

HEK293T cells, GSDMD co-immunoprecipitated with TRIM21 but not with WWP2, a negative interacting protein on the list (Fig. 1a, b). In addition, the isothermal titration calorimetry (ITC) measurement showed that GSDMD directly bound TRIM21($K_d = 1.63 \times 10^{-5}$ M, $\Delta H = -117.9$ kJ mol^{-1}, $\Delta S = -374$ J mol^{-1}) but not WWP2 (negative control) in vitro (Fig. 1c). Interestingly, the co-IP result revealed that TRIM21 interacted not only with the full-length GSDMD, but also with the N-terminus (residues 1–144 or 1–176) and the C-terminus (Fig. 1d, e). The association between TRIM21 and the cleaved-GSDMD fragments (1–275 or 276–484) was confirmed in HEK293T cells transfected with or without LPS (Fig. 1f). Further co-immunoprecipitation (co-IP) experiments in mouse primary BMDMs revealed that endogenous GSDMD as well as its N-terminus could interact with TRIM21 during pyroptosis (Fig. 1g). Therefore, the interaction between TRIM21 and GSDMD may be mediated by intrinsically disordered regions (Fig. S1a) that are present between GSDMD-N and GSDMD-C [24]. Overall, the above results suggest that TRIM21 interacts with both full-length GSDMD and cleaved GSDMD fragments.

TRIM21 binds GSDMD via its PRY-SPRY domain

Similar to other TRIM family members, TRIM21 contains an N-terminal RING-finger domain, a B-box domain (BBOX), a coiled-coil (CC) domain, and a C-terminal PRY-SPRY domain [20, 22, 23]. To further identify the domains responsible for the interaction with GSDMD, we constructed a series of GFP-tagged TRIM21 mutants and assessed them by co-IP (Fig. 2a). The results showed that ΔCCΔPRY-SPRY (in which the coiled-coil and PRY-SPRY domains were deleted) lost the ability to interact with GSDMD (Fig. 2b). As the PRY-SPRY domain of TRIM21 is essential for its binding to SQSTM1/p62 [23], we reasoned that the PRY-SPRY domain might be crucial for TRIM21 interaction with GSDMD. Considering ΔPRY-SPRY-GFP is around 55 kDa (in which the PRY-SPRY domain was deleted) that might be hidden behind the heavy-chain signal, we constructed the PRY-SPRY-GFP and performed the co-IP experiment with GSDMD, which confirmed the PRY-SPRY domain is necessary and enough for binding with GSDMD (Fig. 2c).

Next, we used the gel-filtration chromatography assay to test whether GSDMD forms a complex with the PRY-SPRY domain of TRIM21 in vitro. After incubating with the PRY-SPRY, the fluorescence signal intensities of GSDMD-mCherry dramatically increased in the high-molecular weight fractions (158–669 kDa) in gel-filtration chromatography (Fig. 2d). The SDS-PAGE and immunoblotting results confirmed that GSDMD protein levels increased in the PRY-SPRY-enriched fractions (Fig. 2e, f). Taken together, these results suggest that the PRY-SPRY domain could directly interact with GSDMD. To further investigate whether GSDMD colocalizes with TRIM21, HEK293T cells were co-transfected with the Orange-GSDMD and the TRIM21-GFP, and then analyzed by confocal microscopy. The results clearly showed that GFP-tagged PRY-SPRY co-localized with the GSDMD-N, similar to the colocalization between full-length TRIM21 and the GSDMD-N, suggesting that the PRY-SPRY domain might play a vital role in GSDMD-mediated pyroptotic cell death (Fig. S1b, c).

TRIM21 enhances the stability of GSDMD independent of its E3 ligase activity

Upon LPS stimulation, TRIM21 protein expression was induced by LPS in a time-dependent manner in iBMDMs; while in the TSZ-induced necroptosis, TRIM21 remained steady (Fig. 3a). To test whether TRIM21 modulates GSDMD stability, the human lung carcinoma A549 cells were transfected with TRIM21-GFP or empty vector for 24 h, and then the transfected cells were treated with the protein synthesis inhibitor cycloheximide (CHX) for increasing times as indicated. Interestingly, TRIM21 significantly induced the half-life of endogenous GSDMD in A549 cells (Fig. 3b). Meanwhile, we also observed that the purified GSDMD protein had an extended half-life in the presence of TRIM21, indicating that TRIM21 promoted GSDMD stability in vitro (Fig. 3c).

Knockdown of TRIM21 by siRNA in HeLa cells strongly reduced GSDMD protein expression levels but had no obvious effects on GSDMD mRNA expression (Fig. S1d). Because TRIM21 is an E3 ubiquitin ligase, we first determined whether the enhanced GSDMD protein stability was due to posttranslational modification by TRIM21. Therefore, iBMDM and HeLa cells were induced to undergo pyroptosis with LPS and Nig. Immunoblotting results showed smear bands with apparent molecular masses of 100-245 kDa, significantly larger than what would be expected from unmodified GSDMD (Fig. S1e, f), suggesting that GSDMD was ubiquitinated in cells. The reconstituted ubiquitination assay results revealed that TRIM21 promoted the ubiquitination of GSDMD in vitro (Fig. S1g). We next sought to investigate whether the effect of TRIM21 on GSDMD stability relied on its E3 ligase activity. When treated with CHX, GSDMD protein had an extended half-life in the presence of TRIM21 or its truncated mutant ΔRING in *TRIM21*$^{-/-}$ cells (Fig. 3d). In contrast, depletion of the PRY-SPRY domain did not alter the half-life of GSDMD, indicating that the GSDMD stability required the binding activity rather than the E3 ligase activity of TRIM21 (Fig. 3d). Collectively, these results show that the PRY-SPRY domain of TRIM21 is critical for the stabilization of GSDMD.

TRIM21 positively regulates GSDMD-dependent pyroptosis

Next, we investigated the physiological roles of TRIM21 in cell pyroptosis. Wild type (WT) or *TRIM21*$^{-/-}$ HeLa cells were first transfected with LPS at different doses or different times. The

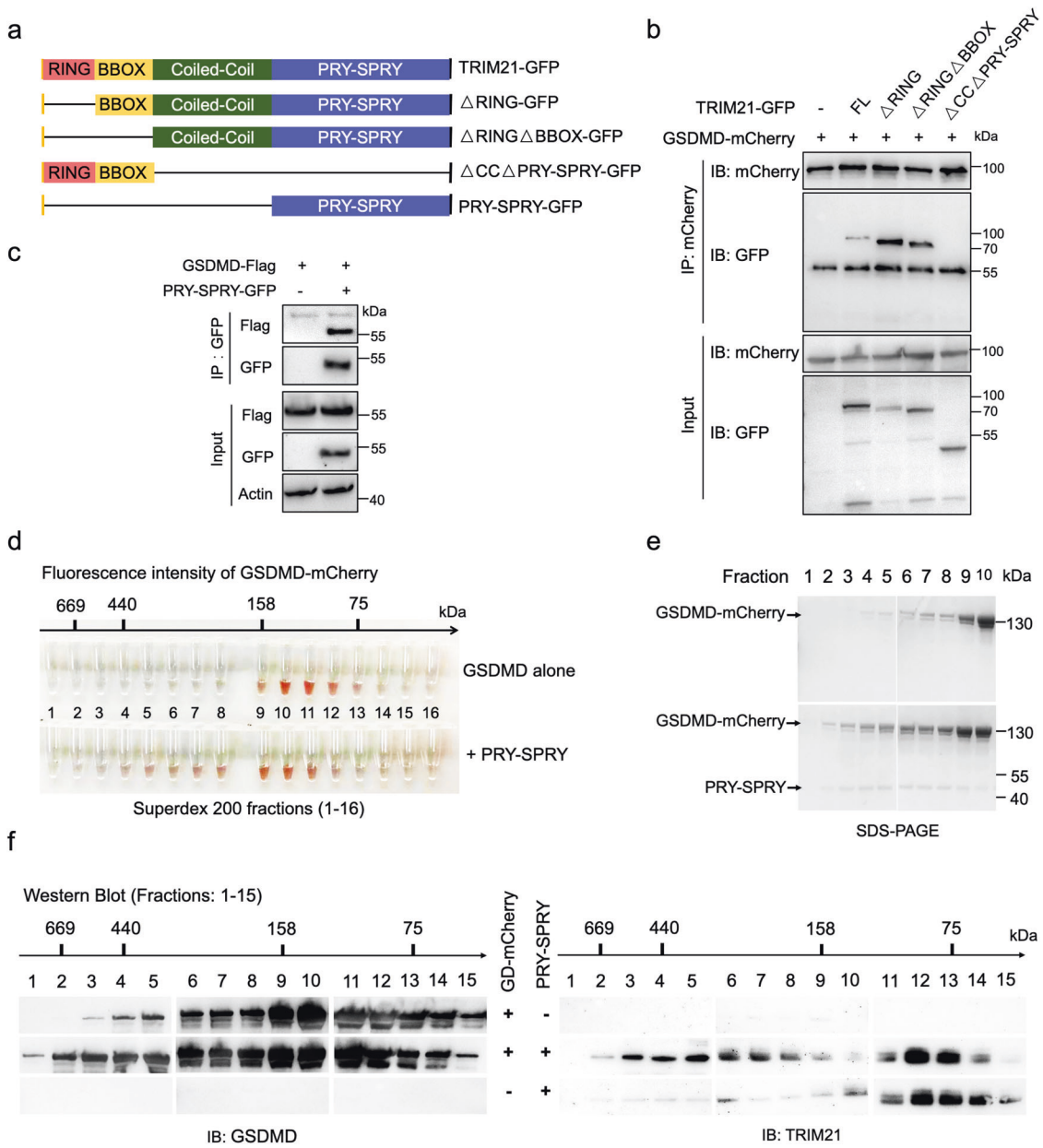

Fig. 2 TRIM21 binds GSDMD via its PRY-SPRY domain. a The schematic diagram of human TRIM21 and its truncated mutants. **b** GFP-tagged TRIM21 or its mutants and GSDMD-mCherry were co-transfected into HeLa cells. Cell lysates were immunoprecipitated with an anti-mCherry antibody and then immunoblotted with the indicated antibodies. **c** The PRY-SPRY domain interacted with GSDMD. PRY-SPRY-GFP and GSDMD-Flag were co-transfected into HEK293T cells. Cell lysates were immunoprecipitated with anti-GFP agarose beads and then immunoblotted with the indicated antibodies. The single-domain antibody used in this assay has no heavy and light chains (KTSM1301, AlpaLife). **d–f** GSDMD physically binds with the PRY-SPRY domain of TRIM21. The purified His-sumo-GSDMD-mCherry was mixed in a total volume of 500 μL reaction buffer (50 mM Tris-HCl, 150 mM NaCl, 2 mM ATP, 10 mM $MgCl_2$, pH 7.4) in the presence or absence of the His-sumo-PRY-SPRY and incubated for 2 h at 37 °C. His-sumo-GSDMD-mCherry shifted to earlier fractions upon the complex formation with the PRY-SPRY. Fluorescence intensities of eluted fractions were shown in (**d**). The arrow indicates the fractions of 669-, 440-, 158-, and 75-kDa standard proteins. **e** SDS-PAGE analysis of the fractions (lanes 1–10) from the analytical gel-filtration column. His-sumo-GSDMD-mCherry shifted to earlier fractions upon the complex formation with the PRY-SPRY. **f** Western blot analysis of the eluted fractions (1–15) was performed with anti-GSDMD and anti-TRIM21 antibodies. All data are representative of three independent experiments.

fluorescence-activated cell sorting (FACS) results showed that pyroptosis of TRIM21-ablated cells was alleviated upon inflammatory stimulations (Fig. S2a). As HeLa cells do not express MD2 and need LPS transfection to activate the noncanonical inflammatory pathway [25], the use of a more physiological system is necessary. Therefore, we used multiple inflammasome stimuli to stimulate mouse primary BMDMs, such as LPS + ATP, LPS + Nig, and LPS + flagellin, which activates NLPR3 or NLRC4 inflammasome, respectively. Firstly, mouse primary BMDM cells isolated from *Trim21*$^{-/-}$ mice were more resistant to each inflammasome stimulator than those isolated from WT mice (Fig. 4a, b). Similar results were detected for living/dead cells by staining with the fluorescence dyes calcein or propidium iodide (PI) in iBMDMs (Fig. 4c). Notably, similar to the WT iBMDMs, *Trim21*$^{-/-}$ cells still showed a pyroptotic morphology after treatments by adding Nig (Fig. 4c).

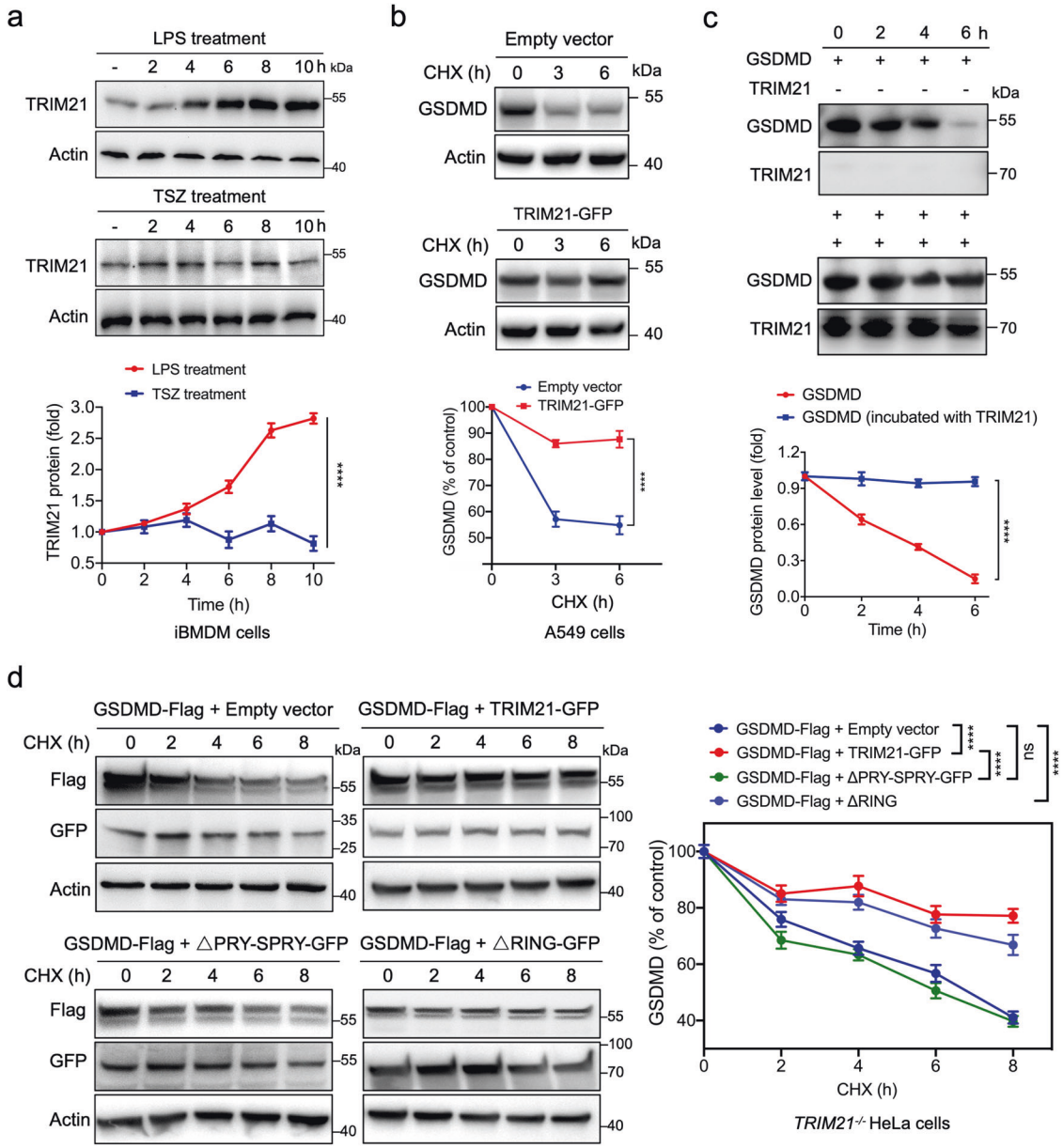

Fig. 3 TRIM21 enhances the stability of GSDMD independent of its E3 ligase activity. a LPS but not TSZ (10 ng/mL TNF-α, 100 nM Smac, and 10 μM ZVAD) stimulation increased the protein levels of TRIM21 in iBMDM cells. **b** TRIM21 increased the half-life of endogenous GSDMD in lung cancer A549 cells, which were transfected with an empty vector or the TRIM21-GFP. 24 h after transfection, cells were treated with 50 μM cycloheximide (CHX) for the indicated periods, followed by immunoblotting analysis and densitometry quantification. **c** 5 μg purified GSDMD was mixed in a total volume of 50 μL reaction buffer in the presence or absence of 5 μg TRIM21. After incubation at 37 °C for 0–6 h, reactions were stopped by adding the 5 × loading buffer containing 4 M urea, and detected by western blot (top). The relative concentration of GSDMD was quantified by densitometry and shown on the bottom. **d** *TRIM21*$^{-/-}$ HeLa cells were transfected with Flag-tagged GSDMD in the presence or absence of GFP-tagged TRIM21 (WT or mutant). Transfected cells were treated with 50 μM CHX for the indicated periods, followed by immunoblotting analysis (left) and densitometry quantification (right). Analysis was performed using the one-way ANOVA (**a**–**d**). Data are shown as mean ± SD (**a**–**d**). ****$P < 0.0001$. All data are representative of three independent experiments.

To further investigate the promotive effect of TRIM21, time-course experiments were conducted in iBMDM and primary BMDM cells. As expected, the results showed that TRIM21 promotes pyroptotic cell death upon LPS plus Nig stimulation with time course in both cell lines (Fig. 4d–f). Similar results were observed in *Trim21*$^{-/-}$ BMDMs (3–9% cytotoxicity) in comparison with WT BMDMs (10-25% cytotoxicity) after treatment with different doses of Nig (Fig. 4g). Moreover, *Trim21*$^{-/-}$ primary BMDMs and WT BMDMs were infected with *S. Typhimurium* at different multiplicity of infection (MOI) or different times. *Trim21*$^{-/-}$ primary BMDMs showed resistance, in comparsion to WT BMDMs, to delayed cell death induced by pathogenic *Salmonella Typhimurium* (SL14028s) (Fig. 4h, i). These results suggested that the pyroptosis of *Trim21*$^{-/-}$ cells was simply delayed, rather than abolished. Next, to determine the effect of TRIM21 on pyroptosis, we assayed the production of IL-1β and IL-18. As shown in Fig. 4j, k, TRIM21 deficiency greatly decreased the biosynthesis of IL-1β and IL-18 in the supernatant of BMDMs upon Nig stimulation.

In addition, LPS plus Nig failed to induce high levels of cell death in *Gsdmd*$^{-/-}$ or *Trim21*$^{-/-}$ iBMDMs (Fig. 5a). Notably, LPS plus Nig-induced cell death was not further inhibited in Gsdmd/Trim21 double knockout cells than in the *Gsdmd*$^{-/-}$

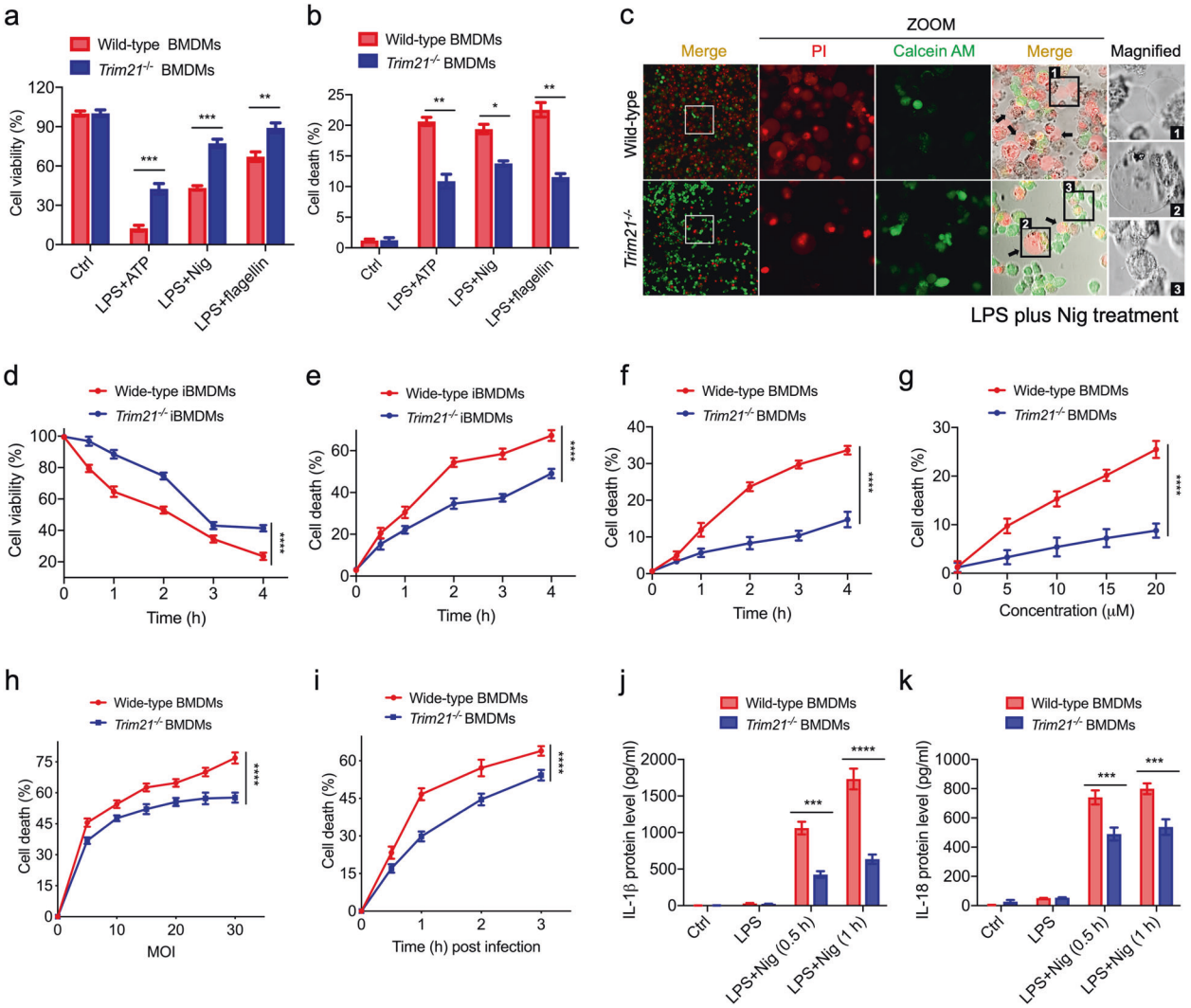

Fig. 4 Depletion of TRIM21 alleviates pyroptosis. a, **b** Primary BMDM cells were isolated from WT and *Trim21*$^{-/-}$ C57BL/6 mice. Cells were primed with 1 μg/mL LPS for 2 h followed by 5 mM ATP or 20 μM Nig or 30 μM flagellin for 30 min. Cell viability (**a**) and cell death (**b**) rates were determined by the Cell Counting Kit-8 (Beyotime) and the LDH Cytotoxicity Assay Kit (Promega), respectively. **c** The alive WT and *Trim21*$^{-/-}$ iBMDM cells were stained by the green calcein, while dead cells were stained by the red PI. Representative data are shown from cells exposed to LPS plus Nig. Arrows indicate the bubbling of pyroptotic cells. Scale bar, 25 μm. **d–f** Time-course effects of TRIM21 on protecting iBMDM cells or primary BMDM cells against 1 μg/mL LPS plus 20 μM Nig-induced pyroptosis. **g** WT and *Trim21*$^{-/-}$ BMDM cells were primed with LPS (1 μg/mL) and treated with Nig at the indicated doses, followed by cell death analysis. **h** Effects of increased concentrations of *S. Typhimurium* (MOI = 0–30) on the cell death after 3 h exposure. **i** WT and *Trim21*$^{-/-}$ BMDM cells were infected by *S. Typhimurium* (MOI = 10) at different time points, followed by cell death analysis. **j**, **k** WT and *Trim21*$^{-/-}$ BMDM cells were primed with LPS (1 μg/mL) and treated with 20 μM Nig at the indicated times, followed by cytokine secretion measurement. The data are the means ± SD of triplicate samples from a representative experiment (*$P < 0.05$; **$P < 0.01$; ***$P < 0.001$; ****$P < 0.0001$). All data are representative of three independent experiments.

iBMDMs (Fig. 5a). Pyroptosis can be assessed by examining the differential solubilities of GSDMD-N and caspases within pyroptotic cells [8]. Therefore, cells were lysed using a buffer containing NP-40 or 4 M urea. We found that the full-length GSDMD protein was dramatically decreased in the insoluble fraction of *Trim21*$^{-/-}$ iBMDMs compared to that of WT iBMDMs during resting state (Fig. 5b, c). Moreover, the results showed that GSDMD-N was significantly decreased in soluble and insoluble fractions after Nig stimulation in *Trim21*$^{-/-}$ iBMDMs (Fig. 5d, e). Therefore, the low abundance of GSDMD-N and cleaved Caspase-3 (p17) appeared to mainly contribute to cell death observed in *Trim21*$^{-/-}$ iBMDMs, which exhibited both apoptotic and pyroptotic features in cell morphologies (Fig. 4c). Moreover, the *Gsdmd*$^{-/-}$ iBMDMs had a higher level of phosphorylated RIP3 and cleaved Caspase-3 than WT and *Trim21*$^{-/-}$ iBMDMs (Fig. 5d, e), similar to the report that inflammasome formation can lead to Caspase-3 dependent apoptosis in the absence of GSDMD [26]. We also observed that knocking out *Trim21* in iBMDMs significantly reduced the levels of GSDMD but not NLRP3 after stimulation, which was in agreement with the dramatically increased cell viability and reduced PI uptake (Fig. 4c). In response to NLRP3 activators, *Trim21*$^{-/-}$ iBMDMs still underwent cell death that was dependent on Caspase-1 and GSDMD-N activation, as the Nig-induced cell death was blocked by treatment with VX-765, a selective inhibitor of Caspase-1 (Fig. S2b). However, both *Gsdmd*$^{-/-}$ and *Gsdmd*$^{-/-}$ *Trim21*$^{-/-}$ iBMDMs might undergo apoptosis in a delayed fashion, and showed a significantly compensatory increase after VX-765 treatment (Fig. S2b). Together, these observations suggested that deficiency of TRIM21 could attenuate pyroptotic cell death through regulating GSDMD.

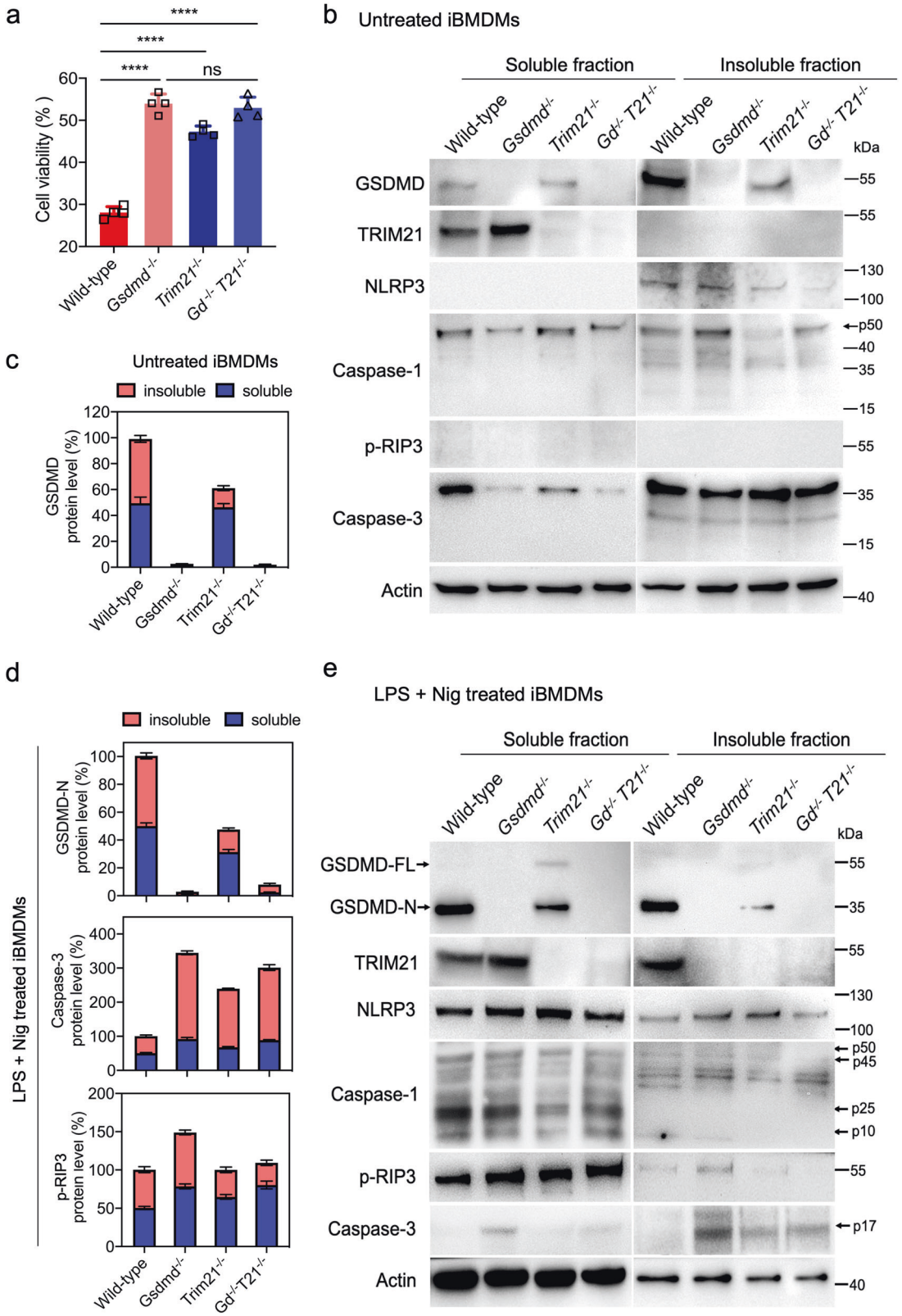

TRIM21 promotes GSDMD-N aggregation during pyroptosis

To further understand the regulatory mechanism of TRIM21 in pyroptotic cell death, we analyzed TRIM21-GFP reconstituted *TRIM21*$^{-/-}$ cells using gel-filtration chromatography. TRIM21 shifted from dimer or low-order oligomers to high-order oligomers or aggregation upon LPS plus Nig treatment (Fig. S2c). Since the oligomerization of GSDMD-N is required for pyroptosis [8, 14, 27], we wonder whether TRIM21 could affect GSDMD oligomerization status

Fig. 5 Depletion of TRIM21 reduces GSDMD-N upon inflammatory stimulation. a WT, *Gsdmd*$^{-/-}$, *Trim21*$^{-/-}$, and *Gsdmd*$^{-/-}$ *Trim21*$^{-/-}$ iBMDM cells were with 1 μg/mL LPS for 2 h followed by 20 μM Nig. *Gd*$^{-/-}$ *T21*$^{-/-}$ denotes double knockout *Gsdmd*$^{-/-}$ *Trim21*$^{-/-}$. Cell death was measured by the LDH Cytotoxicity Assay Kit (Promega). The data are the means ± SD of triplicate samples from a representative experiment (****$P < 0.0001$; ns no significance). **b–e** Immunoblotting analysis of the protein expression levels (TRIM21, GSDMD, NLRP3, Caspase-1, p-RIP3, and Caspase-3) in WT, *Gsdmd*$^{-/-}$, *Trim21*$^{-/-}$, and *Gsdmd*$^{-/-}$ *Trim21*$^{-/-}$ iBMDM cell lines treated with (**e**) or without (**b**) LPS plus Nig as described in (**a**). Quantifications of the results for GSDMD, GSDMD-N, Caspase-3, and p-RIP3 were shown in (**c**) (related to **b**) and (**d**) (related to **e**). The soluble part contained cytoplasmic proteins. The insoluble part contained proteins in the membranes, cell organelles, and nuclei. All the proteins were extracted by the Soluble & Insoluble Protein Extraction Kit (Sangon Biotech, China). p50, pro-caspase-1; p10 and p25, cleaved-caspase-1. p17, cleaved-caspase-3. All data are representative of three independent experiments.

in vitro. Therefore, HA-GSDMD was transfected with or without TRIM21-GFP into *TRIM21*$^{-/-}$ cells. The results showed that the size and concentration of GSDMD-N oligomers increased with the expression levels of TRIM21, suggesting that TRIM21 can promote the formation of high-order oligomers of GSDMD-N in LPS plus Nig-treated cells (Fig. 6a). Next, we investigated the effect of TRIM21 on GSDMD-N oligomerization in primary BMDMs when induced with Nig or flagellin. The results showed that TRIM21 deficiency decreased the GSDMD-N oligomerization during pyroptosis (Fig. 6b). Compared with the empty vector, deletion of the RING domain partially decreased TRIM21-induced pyroptotic cell death in HeLa cells, while deletion of the PRY-SPRY domain nearly abolished the activity of TRIM21 (Fig. 6c). This result suggested that the PRY-SPRY domain but not the RING domain of TRIM21 is critical for pyroptosis regulation. Moreover, both the PRY-SPRY and full-length TRIM21 promoted cell death upon LPS stimulation, indicating that the PRY-SPRY could directly interact with GSDMD, thus promoting pyroptotic cell death (Fig. 6d). In vitro incubation of GSDMD with or without the PRY-SPRY suggested that the PRY-SPRY promoted the formation of GSDMD-N oligomer, which was resistant to 4 M urea (Fig. 6e). These data indicated that TRIM21 could promote GSDMD-N oligomerization and therefore trigger pyroptotic cell death.

TRIM21 deficiency ameliorates LPS-induced inflammation and DSS-induced colitis

The low concentration (5 mg/kg) LPS-induced shock model and high concentration (50 mg/kg) LPS-induced sepsis model [28] were used to confirm the physiological functions of TRIM21 on GSDMD. Firstly, 5 mg/kg LPS-injected WT mice displayed rapid hypothermia within 2 h after injection and had an average body temperature of 26.3 °C after 6 h, whereas the body temperatures of LPS-injected *Trim21*$^{-/-}$ mice did not drop below 33.9 °C (Fig. S2d). The ameliorated inflammatory response in LPS-injected *Trim21*$^{-/-}$ mice was further emphasized by a significant reduction in serum IL-1β, IL-6, and monocyte chemoattractant protein-1 (MCP-1) levels (Fig. S2e), which are vital cytokines associated with pro-inflammatory response [28, 29]. To check whether the in vivo effect of TRIM21 was due to GSDMD-N inhibition, we compared survival rate and the serum levels of IL-1β and IL-18 in *Gsdmd*$^{-/-}$, *Trim21*$^{-/-}$, and WT mice in the presence or absence of 50 mg/kg LPS. Whereas the high concentration of LPS killed 10 of 10 WT mice after 18 h, all *Gsdmd*$^{-/-}$ and 2 of 7 *Trim21*$^{-/-}$ mice survived (Fig. 7a). *Gsdmd*$^{-/-}$ mice, as predicted, produced little IL-1β and IL-18 (Fig. 7b). Although *Trim21*$^{-/-}$ mice secreted more IL-1β and IL-18 than *Gsdmd*$^{-/-}$ mice, the serum levels of IL-1β and IL-18 cytokines in *Trim21*$^{-/-}$ mice was lower than those in WT mice (Fig. 7b). The protective effects of Trim21 deletion were due to the downregulation of GSDMD-N, because GSDMD-N but not the cleaved-caspases was minimally expressed in kidney and lung tissues of LPS-injected *Trim21*$^{-/-}$ mice, especially in the insoluble fractions (Fig. 7c–e). These data demonstrate that Trim21 deficiency ameliorates LPS-induced inflammation by inhibiting GSDMD-dependent pyroptosis.

Because GSDMD is expressed in immune cells and intestinal epithelial cells [30], a DSS-induced colitis model was further used to analyze the function of TRIM21 [31]. As shown in Fig. 7f, *Trim21*$^{-/-}$ mice showed 100% survival after DSS treatment, whereas WT mice only showed a 20% survival rate after 9 days. Significant body weight loss was observed in WT mice; however, this was remarkably alleviated in *Trim21*$^{-/-}$ mice at day 7 after DSS treatment (Fig. 7g). Moreover, the colons of *Trim21*$^{-/-}$ mice were longer than those of WT mice administered with DSS (Fig. 7h, i). Hematoxylin and eosin staining revealed severe vascular ruptures within focal areas with extensive ulceration. Necrotic lesions were observed in WT mice, whereas these ulcerations and lesions did not appear in DSS-treated *Trim21*$^{-/-}$ mice (Fig. 7j). When compared to those of WT mice, the colons of *Trim21*$^{-/-}$ mice exhibited significantly increased Ki67 expression, suggesting that the intestinal epithelial cells of *Trim21*$^{-/-}$ mice were more proliferative and could more effectively repair mucosal damage (Fig. 7k). Also, GSDMD-N was markedly down-regulated in *Trim21*$^{-/-}$ mice compared to WT mice (Fig. 7l). Collectively, these results indicate that TRIM21 deficiency alleviates DSS-induced colitis.

DISCUSSION

Improper activation of pyroptosis can induce sepsis, metabolic disease, ischemia-reperfusion, and atherosclerosis [32]. The key executioner of pyroptosis, GSDMD, oligomerizes and forms pore-like structures on the plasma membranes upon inflammatory stimulation [6, 7]. Our current study identified TRIM21 as a new regulator for GSDMD. TRIM21 directly interacted with the full-length GSDMD and GSDMD-N via its PRY-SPRY domain. TRIM21 formed a stable complex with GSDMD and promotes GSDMD-N aggregation during pyroptotic cell death, consistent with the previous report that TRIM21 could form high-molecular-weight oligomers under stress conditions [33]. Furthermore, *Trim21* knockdown protected BMDM cells from these pyroptotic signals. In vivo experiments confirmed that TRIM21 deficiencies protected mice from LPS-induced sepsis and DSS-induced colitis. Thus, as a decisive factor, TRIM21 maintained the stable expression level of GSDMD by interacting through its PRY-SPRY domain under physiological conditions. When GSDMD is processed by inflammatory caspases and cleaved into GSDMD-N and GSDMD-C fragments, the PRY-SPRY domain of TRIM21 promotes the formation of GSDMD-N polymers, which accelerates pyroptotic cell death. Because the pore-like structure formed by GSDMD is critical for the release of inflammatory cytokines and lytic cell death [6, 7], TRIM21 silencing might be a critical therapeutic approach for autoimmune disease treatment.

Protein ubiquitination is critical for the immune system to sense and fight infections [34]. E3 ligases can mediate K63-linked ubiquitination, which activates the cytosolic RNA sensor RIG-I and MAVS [35–38], as well as the atypical monoubiquitination of the cytosolic DNA sensor cGAS, resulting in a marked increase in its dimerization, DNA-binding activity, and cGAMP production [39]. It has been reported that TRIM21 enhances Keratin 17 (K17) stability via ubiquitination through K63-linkage [40]. The function of TRIM proteins is closely related to its structure domain. For instance, TRIM25 interacts with a wide variety of RNAs through its PRY-SPRY domain [41], and three amino acid substitutions in the PRY-SPRY domain of human TRIM5α allow it to restrict HIV-1 [42]. In this study, we observed that TRIM21-induced GSDMD ubiquitination in vitro, whereas TRIM21 stabilized GSDMD independent of its

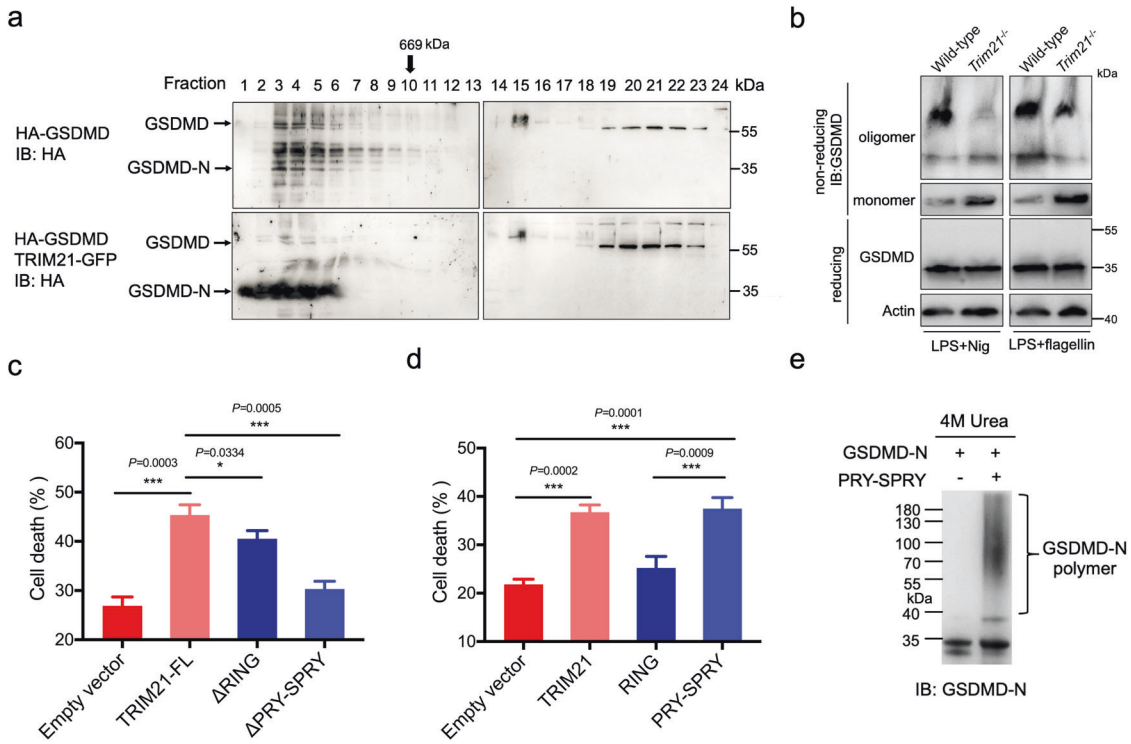

Fig. 6 The PRY-SPRY domain of TRIM21 promotes GSDMD-N oligomerization and cell death. a TRIM21 promoted GSDMD-N oligomerization. *TRIM21*$^{-/-}$ HeLa cells were transfected with the indicated constructs. 16 h later, cells were transfected with LPS and treated with Nig. Cells were lysed by the RIPA buffer (containing 1% Triton X-100 and 0.1% SDS) and then lysates were fractionated by gel-filtration chromatography (Superpose 6 column, MW marker at the top) and followed by immunoblotting analysis. **b** WT and *Trim21*$^{-/-}$ BMDM cell lines were treated with LPS plus 20 μM Nig or 30 μM Flagellin for 4 h. Cells were lysed in IP lysis buffer and then mixed with loading buffer with or without β-mercaptoethanol and subjected to immunoblotting analysis. **c**, **d** *TRIM21*$^{-/-}$ HeLa cells reconstituted with TRIM21 WT or its mutants were transfected with 1 μg/mL LPS for 4 h followed by 20 μM Nig. Cell death was determined by the CytoTox96 assay. **e** PRY-SPRY domain of TRIM21 and GSDMD-N were expressed in *E. coli* BL21 (DE3) cells and further purified by the Ni-affinity chromatography. 5 μg purified GSDMD-N protein (residues 48–265) was mixed in a total volume of 50 μL reaction buffer in the presence or absence of 5 μg His-sumo tagged PRY-SPRY. After incubation at 37 °C for 2 h, reactions were stopped by adding a 5 × loading buffer containing 1% SDS or 4 M urea. GSDMD-N was measured by an anti-cleaved N-terminal GSDMD antibody (Abcam, ab215203). All the data are the means ± SD of triplicate samples from a representative experiment of three independent experiments. *$P < 0.05$; **$P < 0.01$; ***$P < 0.001$.

RING domain. The PRY-SPRY domain alone could promote GSDMD-N aggregation and aggravated pyroptotic cell death.

TRIM21 binds normal serum IgG, anti-TRIM21 autoantibodies, and SQSTM1/p62 via its PRY-SPRY domain [33, 43], and recognizes antibody-coated viruses, thereby resulting in the proteasome-dependent degradation of the antigenic target [44]. Our investigation of TRIM21 mediating GSDMD-dependent pyroptotic cell death expanded the known function of TRIM21 against infections. In the early stages of infection, antibodies were delivered efficiently to the cytoplasm and were recruited by the cytosolic Fc receptor TRIM21, resulting in the proteasome-dependent degradation of the antigenic target [44]. When the infection was in the latent stage, our study showed that TRIM21 primarily resisted danger signals by positively regulating cell pyroptosis. Furthermore, we detected the C-terminus of TRIM21 (at around 35 kDa) in both stimulated HeLa cells and DSS-treated mouse tissues (Figs. 7l, S2c). However, how TRIM21 is cleaved upon inflammatory stimulation and whether the truncation regulates GSDMD-induced pyroptosis need to be further investigated. Because GSDMD and other gasdermin family proteins (GSDMA, GSDMB, GSDMC, or DFNA5) share the pore-forming activity with the lipid bilayer and can induce extensive cell death [8, 14, 45], it remains unclear whether TRIM21 is a universal binding protein required for the stabilization and activation of other gasdermin family proteins. Moreover, TRIM21 might also interact with other pore-forming proteins like MLKL to regulate necroptosis. Taken together, our findings open a new avenue for future studies to elucidate the complexities of the homeostatic control of pyroptotic cell death.

MATERIALS AND METHODS

Mice

All animal experiments were performed in accordance with the NIH Guide for the Care and Use of Laboratory Animals, with the approval of the Scientific Investigation Board of School of Life Sciences, Fudan University (2019-JS-011). Female C57BL/6 mice with a *Trim21*$^{-/-}$ genotype were generated by the Institute of Biomedical Science, East China Normal University (Shanghai, China) using TALEN technology, as described previously [46]. Tail clips were extracted from offsprings, and the primers used for TRIM21 genotyping were forward: 5′-AGAGGCTCCTGTCATTC AG-3′ and reverse: 5′-CTTTGCCTCTGCTGCTGAG-3′. *Gsdmd*$^{-/-}$ mice were gifted from Dr. Z. Lin at Nanjing University. C57BL/6 mice were obtained from the SLAC Laboratory Animal Co. (Shanghai, China). Mutant alleles were backcrossed with C57BL/6 mice for more than six generations. Mice used in the experiment were at 6 to 8 weeks of age and 20 to 25 g of weight.

LPS-induced inflammation

First, mice were injected intraperitoneally with 5 mg/kg *E. coli* O111:B4 LPS (Sigma, USA). The injection volume for all experiments was 200 μL with sterile PBS. Mice were monitored by a rectal thermometer every 2 h and were sacrificed 18 h after LPS injection. Serum was prepared from coagulated blood centrifuged at 2000 × *g* for 90 s at room temperature for further ELISA analysis (IL-1β, IL-6, IL-18, and MCP-1). Second, mice were

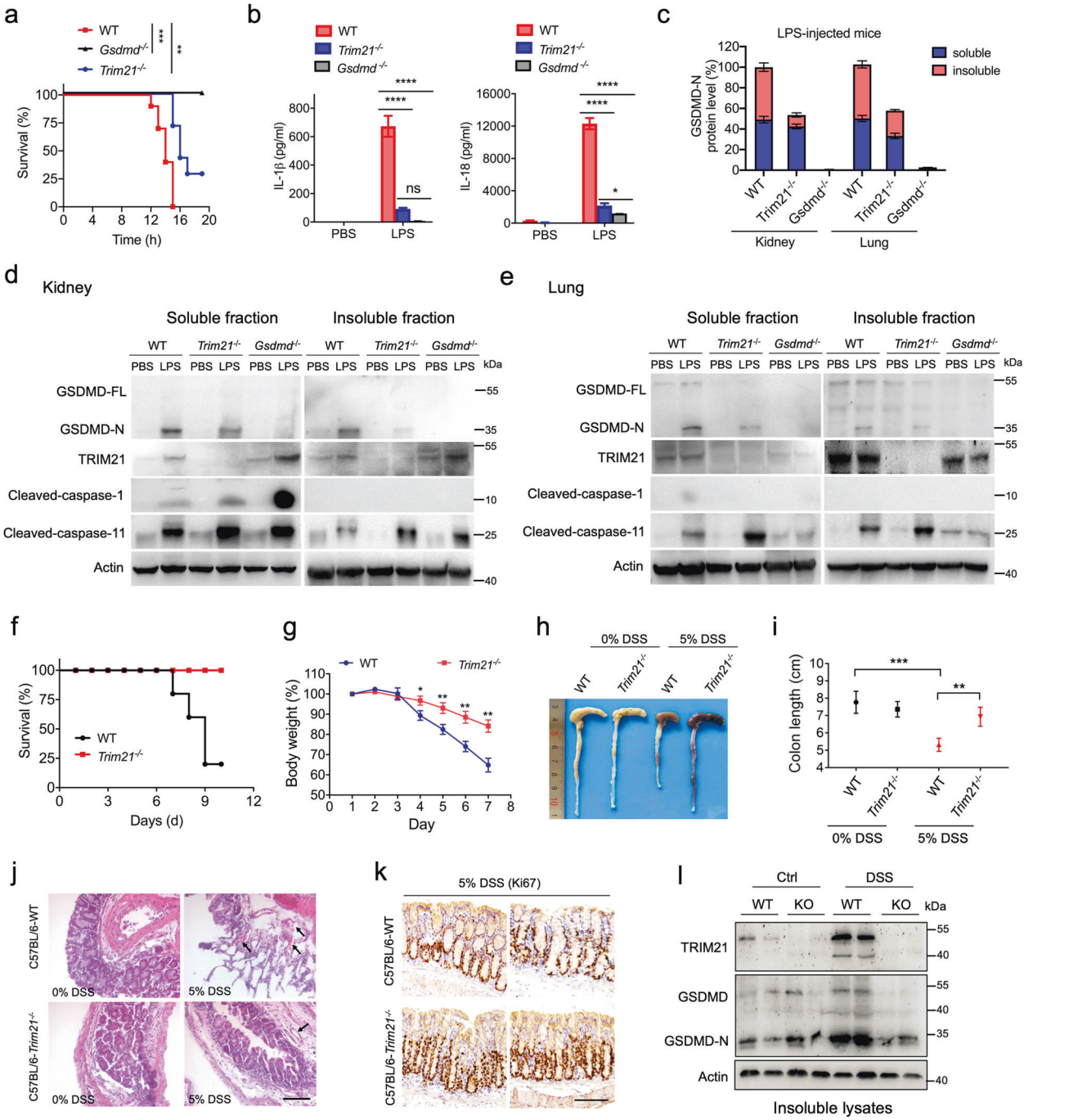

Fig. 7 TRIM21 deficiency ameliorates LPS-induced inflammation and DSS-induced colitis. a Kaplan–Meier survival plot for WT ($n = 10$), *Trim21*$^{-/-}$ ($n = 7$), and *Gsdmd*$^{-/-}$ mice ($n = 7$) intraperitoneally injected with PBS or LPS (50 mg/kg). **b** IL-1β and IL-18 concentrations in the serum from WT, *Trim21*$^{-/-}$ and *Gsdmd*$^{-/-}$ mice. **c–e** Representative images of immunoblot analysis of the indicated proteins in soluble and insoluble fractions of kidney and lung tissues from WT, *Trim21*$^{-/-}$, and *Gsdmd*$^{-/-}$ mice (**d**, **e**). The relative concentration of GSDMD-N in LPS-injected groups was quantified by densitometry, and the results were shown in (**c**). **f** Kaplan–Meier survival plot for WT and *Trim21*$^{-/-}$ mice ($n = 5$ mice per group) given 5% DSS in their drinking water for 7 days, followed by regular drinking water. **g** Body weights of mice treated as in (**a**) were recorded on different days. **h**, **i**, Mice were killed on day 8. The macroscopic appearance (**h**) and colon lengths (**i**) of the mice were measured. **j** Histopathological changes in colon tissues were examined by H&E staining. Black arrows represent vascular rupture. Scale bar, 50 μm. **k** Immunohistochemistry (IHC) analysis of Ki67 expression in normal and *Trim21*$^{-/-}$ colon tissues. Scale bar, 100 μm. **l** GSDMD and TRIM21 protein expression levels in colon tissues were analyzed by immunoblotting. The data are the means ± SD of triplicate samples from a representative experiment. *$P < 0.05$; **$P < 0.01$; ***$P < 0.001$; ****$P < 0.0001$. All data are representative of three independent experiments.

injected with 50 mg/kg LPS. For the survival study, mice were constantly monitored for 20 h, and then euthanized by cervical dislocation. In a separate experiment, mice were sacrificed on 8 h after LPS injection, followed by ELISA assay from serum samples and western blot analysis from kidney and lung tissues.

DSS-induced colitis

Colitis was induced by adding 5% DSS (Sangon Biotech, China) to the drinking water of the mice. After 7 days, DSS was replaced with normal drinking water. For the survival study, mice were constantly monitored for 10 days, and then euthanized by cervical dislocation. In a separate

experiment, mice were weighed daily and sacrificed on day 8. The lengths of the colons were measured, and the sections close to the rectum were collected for protein extraction and histological analysis.

Cells

HeLa, HEK293T, and iBMDM cells were cultured in high-glucose DMEM supplemented with 10% (v/v) FBS (Hyclone, UK), and A549 cells were cultured in RPMI 1640 medium supplemented with fetal bovine serum at 37 °C. HeLa and HEK293T cell lines were purchased from ATCC (Manassas, USA). All cells were grown at 37 °C in a 5% CO_2 incubator (Thermo Fisher, USA). Cells were primed with 1 μg/mL LPS (Sigma, USA), and then stimulated with 20 μM nigericin (MedChemExpress, USA), 5 mM ATP (MedChemExpress) or transfected with 30 μM flagellin (Invitrogen, USA) to induce pyroptosis. PolyJet (Signage, USA) or Lipofectamine RNAiMAX (Invitrogen, USA) was used for the transfection of corresponding LPS, plasmids or siRNAs into cells.

Isolation and culturing of primary bone-marrow-derived macrophages (BMDMs)

Trim21$^{-/-}$, *Gsdmd*$^{-/-}$, and WT mice were euthanized in accordance with institutional animal ethics guidelines. Bone marrow-derived macrophages (BMDMs) were isolated and cultured as described previously [47, 48]. Notably, 10 ng/mL M-CSF and 10% FBS was included in the conditioned medium while primary BMDMs were being differentiated. No differentiation or viability differences were observed among *Trim21*$^{-/-}$, *Gsdmd*$^{-/-}$, and WT BMDMs.

Cytotoxicity and cell viability assays

Cell death and cell viability were determined by the lactate dehydrogenase (LDH) release assay using the CytoTox 96 Non-Radioactive Cytotoxicity Assay kit (Promega) and Cell Counting Kit-8 (Beyotime), respectively, according to the manufacturer's instructions. Luminescence and absorbance were measured on a SpectraMax M5 plate reader.

Plasmids

TRIM21 cDNA was kindly provided by Dr. Jiahuai Han (Xiamen University, China), and cloned into the pcDNA3.1-HA and pEGFP-N1 vectors, respectively. HA-tagged GSDMD, ZsYellow tagged GSDMD, and mCherry-tagged GSDMD were subcloned from pcDNA3.1-GSDMD-Flag as described previously [15]. Truncated mutants of TRIM21 or GSDMD were amplified from the full-length TRIM21 and GSDMD, which were then subcloned into the pEGFP-N1 or pmCherry-N1 vectors. All constructs were confirmed by DNA sequencing.

Flow cytometry assay

HeLa cells were collected using 0.25% trypsin-EDTA and washed in PBS. The cells were resuspended in PBS and incubated at RT for 5 min with 5 μg/mL propidium iodide (BD Biosciences, USA) according to the manufacturer's protocol. The pyroptotic cells were analyzed using a FACScan flow cytometer (BD Biosciences).

Protein preparation, immunoprecipitation, and immunoblotting analysis

For ubiquitination analysis, the total cellular protein was isolated with a lysis buffer (50 mM Tris-HCl, pH 7.5, 150 mM NaCl, 1 mM EDTA, 2% SDS, and complete protease inhibitor cocktail tablets). For IP, whole-cell extracts were lysed in a buffer composed of 50 mM Tris-HCl (pH 7.5), 150 mM NaCl, 1 mM EDTA, and 1% NP-40 containing protease inhibitors. After prewashing with corresponding IgG (Santa Cruz Biotechnology) and protein G agarose immunoprecipitation reagent (Beyotime Inst Biotech, China) for 1 h at 4 °C, cell lysates were incubated with the appropriate primary antibody overnight at 4 °C followed by 4 h incubation with protein A/G agarose beads. The beads were washed five times with the lysis buffer and were eluted in a 5 × SDS/PAGE loading buffer for immunoblotting. For immunoblotting analysis, cells were lysed with a buffer (50 mM Tris-HCl, pH 7.5, 150 mM NaCl, 1 mM EDTA and 1% Triton X-100) supplemented with protein inhibitors (Roche, Switzerland). The cell lysates were incubated with the following antibodies: anti-HA (Proteintech, 51064-2-AP), anti-FLAG (Proteintech, 20543-1-AP), anti-His (Proteintech, 66005-1-Ig), anti-GFP (Proteintech, 66002-1-Ig), anti-mCherry (Abcam, 50430-2-AP), anti-human GSDMD (Abcam, ab210070), anti-GSDMD (from Dr. J. Lieberman), anti-GSDMD-N (Abcam, ab215203), anti-mouse GSDMD (Abcam, ab209845), anti-TRIM21 (Abcam, ab207728), anti-Caspase-1 (Cell Signaling Technology, 24232), anti-Caspase-3 (Cell Signaling Technology,14220), anti-Caspase-11 (abcam, ab180673), anti-NLRP3 (Wanleibio, WL02635), and anti-p-RIP3 (abcam, ab222320). Western blotting was performed in three independent experiments.

Isothermal titration calorimetry (ITC) assay

The ITC measurement was performed using MicroCal ITC200 (GE, USA). 30 μM TRIM21 or WWP2 was titrated with 150 μM GSDMD. Protein samples were sterile filtered before degassing, and all solutions were degassed under vacuum to eliminate air bubble formation inside the calorimeter cell.

Recombinant protein expression, purification, and in vitro ubiquitination assay

The full-length GSDMD, TRIM21, ubiquitin, E1, and E2 (UbcH5A) were subcloned into the pSMT3 vector with a His-SUMO tag. All proteins were expressed in *E.coli* BL21 (DE3) cells and further purified by Ni-affinity chromatography. After cleavage of the His-SUMO tag with the Ulp1 enzyme, the target proteins were reapplied to the Ni-affinity column. Fractions throughout the column were collected, concentrated, and then purified with gel-filtration chromatography (Superdex 75 10/300 or Superdex 200 16/600, GE, USA). All proteins were in a buffer containing 20 mM Tris-HCl, 150 mM NaCl, 2 mM DTT, pH 8.0. For the in vitro ubiquitination assay, 5 μg purified GSDMD was mixed in a total volume of 50 μL containing 5 mM ATP, 5 mM $MgCl_2$, 5 μg ubiquitin, and 1 μg E1 and E2 enzymes in the presence or absence of TRIM21. After incubation at 37 °C for 1 h, reactions were stopped by adding the 5× loading buffer and analyzed by western blotting using an anti-GSDMD antibody.

Confocal analysis

Images were captured using a Zeiss 880 laser scanning confocal microscope and analyzed using a Zeiss Zen software. Manders' overlap coefficient was calculated using ImageJ. All images are representative of at least three independent experiments.

Statistical analysis

Each experiment was performed at least three times. All experiment data were analyzed using GraphPad Prism 8.0 (GraphPad software Inc. USA) and were presented as the mean ± SD. Statistical analysis was performed using Student's *t* test, one-way ANOVA or two-way ANOVA. A value of $P < 0.05$ was considered statistically significant.

DATA AVAILABILITY

All data needed to evaluate the conclusions in the paper are present in the paper and/or the Supplementary Materials. Additional data related to this paper may be requested from the corresponding author.

REFERENCES

1. Galluzzi L, Vitale I, Aaronson SA, Abrams JM, Adam D, Agostinis P, et al. Molecular mechanisms of cell death: recommendations of the Nomenclature Committee on Cell Death 2018. Cell Death Differ. 2018;25:486–541.
2. Kovacs SB, Miao EA. Gasdermins: effectors of pyroptosis. Trends Cell Biol. 2017;27:673–84.
3. Li J, McQuade T, Siemer AB, Napetschnig J, Moriwaki K, Hsiao YS, et al. The RIP1/RIP3 necrosome forms a functional amyloid signaling complex required for programmed necrosis. Cell. 2012;150:339–50.
4. Mompeán M, Li W, Li J, Laage S, Siemer AB, Bozkurt G, et al. The structure of the necrosome RIPK1-RIPK3 core, a human hetero-amyloid signaling complex. Cell. 2018;173:1244–53.e1210.
5. Green DR. The coming decade of cell death research: five riddles. Cell. 2019;177:1094–107.
6. Kayagaki N, Stowe IB, Lee BL, O'Rourke K, Anderson K, Warming S, et al. Caspase-11 cleaves gasdermin D for non-canonical inflammasome signalling. Nature. 2015;526:666–71.
7. Shi J, Zhao Y, Wang K, Shi X, Wang Y, Huang H, et al. Cleavage of GSDMD by inflammatory caspases determines pyroptotic cell death. Nature. 2015;526:660–5.
8. Liu X, Zhang Z, Ruan J, Pan Y, Magupalli VG, Wu H, et al. Inflammasome-activated gasdermin D causes pyroptosis by forming membrane pores. Nature. 2016;535:153–8.
9. Martinon F, Tschopp J. Inflammatory caspases: linking an intracellular innate immune system to autoinflammatory diseases. Cell. 2004;117:561–74.
10. Man SM, Kanneganti TD, Gasdermin D. the long-awaited executioner of pyroptosis. Cell Res. 2015;25:1183–4.

11. Ruan J, Xia S, Liu X, Lieberman J, Wu H. Cryo-EM structure of the gasdermin A3 membrane pore. Nature. 2018;557:62–7.
12. Chen X, He WT, Hu L, Li J, Fang Y, Wang X, et al. Pyroptosis is driven by non-selective gasdermin-D pore and its morphology is different from MLKL channel-mediated necroptosis. Cell Res. 2016;26:1007–20.
13. Wright JA, Bryant CE. The killer protein Gasdermin D. Cell Death Differ. 2016;23:1897–8.
14. Ding J, Wang K, Liu W, She Y, Sun Q, Shi J, et al. Pore-forming activity and structural autoinhibition of the gasdermin family. Nature. 2016;535:111–6.
15. Kuang S, Zheng J, Yang H, Li S, Duan S, Shen Y, et al. Structure insight of GSDMD reveals the basis of GSDMD autoinhibition in cell pyroptosis. Proc Natl Acad Sci USA. 2017;114:10642–7.
16. Liu Z, Wang C, Yang J, Zhou B, Yang R, Ramachandran R, et al. Crystal structures of the full-length murine and human gasdermin D reveal mechanisms of autoinhibition, lipid binding, and oligomerization. Immunity. 2019;51:43–9.e44.
17. Orning P, Weng D, Starheim K, Ratner D, Best Z, Lee B, et al. Pathogen blockade of TAK1 triggers caspase-8-dependent cleavage of gasdermin D and cell death. Science. 2018;362:1064–9.
18. Evavold CL, Ruan J, Tan Y, Xia S, Wu H, Kagan JC. The pore-forming protein gasdermin D regulates interleukin-1 secretion from living macrophages. Immunity. 2018;48:35–44.e36.
19. Ruhl S, Shkarina K, Demarco B, Heilig R, Santos JC, Broz P. ESCRT-dependent membrane repair negatively regulates pyroptosis downstream of GSDMD activation. Science. 2018;362:956–60.
20. Hatakeyama S. TRIM family proteins: roles in autophagy, immunity, and carcinogenesis. Trends Biochem Sci. 2017;42:297–311.
21. Oke V, Wahren-Herlenius M. The immunobiology of Ro52 (TRIM21) in autoimmunity: a critical review. J Autoimmun. 2012;39:77–82.
22. Xue B, Li H, Guo M, Wang J, Xu Y, Zou X, et al. TRIM21 promotes innate immune response to RNA viral infection through Lys27-linked polyubiquitination of MAVS. J Virol. 2018;92.
23. Pan JA, Sun Y, Jiang YP, Bott AJ, Jaber N, Dou Z, et al. TRIM21 ubiquitylates SQSTM1/p62 and suppresses protein sequestration to regulate redox homeostasis. Mol Cell. 2016;61:720–33.
24. Samir P, Kesavardhana S, Patmore DM, Gingras S, Malireddi RKS, Karki R, et al. DDX3X acts as a live-or-die checkpoint in stressed cells by regulating NLRP3 inflammasome. Nature. 2019;573:590–4.
25. Wyllie DH, Kiss-Toth E, Visintin A, Smith SC, Boussouf S, Segal DM, et al. Evidence for an accessory protein function for Toll-like receptor 1 in anti-bacterial responses. J Immunol. 2000;165:7125–32.
26. Rogers C, Erkes DA, Nardone A, Aplin AE, Fernandes-Alnemri T, Alnemri ES. Gasdermin pores permeabilize mitochondria to augment caspase-3 activation during apoptosis and inflammasome activation. Nat Commun. 2019;10:1689.
27. Qiu S, Liu J, Xing F. 'Hints' in the killer protein gasdermin D: unveiling the secrets of gasdermins driving cell death. Cell Death Differ. 2017;24:588–96.
28. Kayagaki N, Warming S, Lamkanfi M, Vande Walle L, Louie S, Dong J, et al. Non-canonical inflammasome activation targets caspase-11. Nature. 2011;479:117–21.
29. Bozza FA, Salluh JI, Japiassu AM, Soares M, Assis EF, Gomes RN, et al. Cytokine profiles as markers of disease severity in sepsis: a multiplex analysis. Crit Care. 2007;11:R49.
30. Aglietti RA, Dueber EC. Recent insights into the molecular mechanisms underlying pyroptosis and gasdermin family functions. Trends Immunol. 2017;38:261–71.
31. Wirtz S, Neufert C, Weigmann B, Neurath MF. Chemically induced mouse models of intestinal inflammation. Nat Protoc. 2007;2:541–6.
32. Shi J, Gao W, Shao F. Pyroptosis: gasdermin-mediated programmed necrotic cell death. Trends Biochem Sci. 2017;42:245–54.
33. Rhodes DA, Isenberg DA. TRIM21 and the function of antibodies inside cells. Trends Immunol. 2017;38:916–26.
34. Jiang X, Chen ZJ. The role of ubiquitylation in immune defence and pathogen evasion. Nat Rev Immunol. 2011;12:35–48.
35. Cadena C, Ahmad S, Xavier A, Willemsen J, Park S, Park JW, et al. Ubiquitin-dependent and -independent roles of E3 ligase RIPLET in innate immunity. Cell. 2019;177:1187–200.
36. Gack MU, Shin YC, Joo CH, Urano T, Liang C, Sun L, et al. TRIM25 RING-finger E3 ubiquitin ligase is essential for RIG-I-mediated antiviral activity. Nature. 2007;446:916–20.
37. Yan J, Li Q, Mao AP, Hu MM, Shu HB. TRIM4 modulates type I interferon induction and cellular antiviral response by targeting RIG-I for K63-linked ubiquitination. J Mol Cell Biol. 2014;6:154–63.
38. Liu B, Zhang M, Chu H, Zhang H, Wu H, Song G, et al. The ubiquitin E3 ligase TRIM31 promotes aggregation and activation of the signaling adaptor MAVS through Lys63-linked polyubiquitination. Nat Immunol. 2017;18:214–24.
39. Seo GJ, Kim C, Shin WJ, Sklan EH, Eoh H, Jung JU. TRIM56-mediated monoubiquitination of cGAS for cytosolic DNA sensing. Nat Commun. 2018;9:613.
40. Yang L, Jin L, Ke Y, Fan X, Zhang T, Zhang C, et al. E3 Ligase Trim21 ubiquitylates and stabilizes keratin 17 to induce STAT3 activation in psoriasis. J Investig Dermatol. 2018;138:2568–77.
41. Sanchez JG, Sparrer KMJ, Chiang C, Reis RA, Chiang JJ, Zurenski MA, et al. TRIM25 binds RNA to modulate cellular anti-viral defense. J Mol Biol. 2018;430:5280–93.
42. Yap MW, Nisole S, Stoye JP. A single amino acid change in the SPRY domain of human Trim5alpha leads to HIV-1 restriction. Curr Biol. 2005;15:73–8.
43. Pan JA, Sun Y, Jiang YP, Bott AJ, Jaber N, Dou Z, et al. TRIM21 ubiquitylates SQSTM1/p62 and suppresses protein sequestration to regulate redox homeostasis. Mol Cell. 2016;62:149–51.
44. James LC, Keeble AH, Khan Z, Rhodes DA, Trowsdale J. Structural basis for PRYSPRY-mediated tripartite motif (TRIM) protein function. Proc Natl Acad Sci USA. 2007;104:6200–5.
45. Wang Y, Gao W, Shi X, Ding J, Liu W, He H, et al. Chemotherapy drugs induce pyroptosis through caspase-3 cleavage of a gasdermin. Nature. 2017;547:99–103.
46. Zhou G, Wu W, Yu L, Yu T, Yang W, Wang P, et al. Tripartite motif-containing (TRIM) 21 negatively regulates intestinal mucosal inflammation through inhibiting TH1/TH17 cell differentiation in patients with inflammatory bowel diseases. J Allergy Clin Immunol. 2018;142:1218–28.e1212.
47. Assouvie A, Daley-Bauer LP, Rousselet G. Growing murine bone marrow-derived macrophages. Methods Mol Biol. 2018;1784:29–33.
48. Pineda-Torra I, Gage M, de Juan A, Pello OM. Isolation, culture, and polarization of murine bone marrow-derived and peritoneal macrophages. Methods Mol Biol. 2015;1339:101–9.
49. Sacks D, Baxter B, Campbell BCV, Carpenter JS, Cognard C, Dippel D, et al. Multisociety consensus quality improvement revised consensus statement for endovascular therapy of acute ischemic stroke. Int J Stroke. 2018;13:612–32.

ACKNOWLEDGEMENTS

We thank Dr. H. Saiyin for the help in mouse tissue IHC experiments. *Gsdmd*$^{-/-}$ HeLa cells and *Gsdmd*$^{-/-}$ iBMDMs are kindly provided by Dr. F. Shao (National Institute of Biological Sciences, China). *Gsdmd*$^{-/-}$ mice are kindly provided by Dr. Z. Lin (Nanjing University, China). WT pathogenic *Salmonella typhimurium* (SL14028s) is kindly provided by Dr. Y. Yao (Shanghai Jiaotong University, China).

AUTHOR CONTRIBUTIONS

JL, XC, and WG conceived and designed the study. WG, YL, XL, SW, PM, ZC, KL, SL, XX, JG, JW, CJ, CD, XL, YL, HH, JL, and HW performed the experiments and analyzed the data. JL and WG analyzed the data and wrote the paper. All authors discussed the results and commented on the paper.

FUNDING

This work was supported by grants from the National Natural Science Foundation of China (82071782, 31670878), the National Key Research and Development Project of China (2016YFA0500600), and the Shanghai Committee of Science and Technology (20XD1400800).

COMPETING INTERESTS

The authors declare no competing interests.

ETHICS APPROVAL

All animal experiments were performed in accordance with the NIH Guide for the Care and Use of Laboratory Animals, with the approval of the Scientific Investigation Board of School of Life Sciences, Fudan University (2019-JS-011).

ADDITIONAL INFORMATION

Supplementary information The online version contains supplementary material available at https://doi.org/10.1038/s41418-021-00867-z.

Correspondence and requests for materials should be addressed to Xiangjun Chen or Jixi Li.